Science Bulletin 67 (2022) 1284–1294

Contents lists available at ScienceDirect

Science Bulletin

journal homepage: www.elsevier.com/locate/scib

Article

Hybrid nanogenerator based closed-loop self-powered low-level vagus nerve stimulation system for atrial fibrillation treatment

Yu Sun [a,d,1], Shengyu Chao [b,c,1], Han Ouyang [c], Weiyi Zhang [b], Weikang Luo [e], Qingbin Nie [d], Jianing Wang [a,d], Changyi Luo [a,d], Gongang Ni [a,d], Lingyu Zhang [a,d], Jun Yang [h,*], Hongqing Feng [b,c,*], Gengsheng Mao [a,d,*], Zhou Li [b,c,f,g,*]

[a] Department of Neurosurgery, General Hospital of Armed Police Forces, Anhui Medical University, Hefei 230032, China
[b] Beijing Key Laboratory of Micro-nano Energy and Sensor, Beijing Institute of Nanoenergy and Nanosystems, Chinese Academy of Sciences, Beijing 101400, China
[c] School of Nanoscience and Technology, University of Chinese Academy of Sciences, Beijing 100049, China
[d] Department of Neurosurgery, The Third Medical Centre, Chinese People's Liberation Army General Hospital, Beijing 100039, China
[e] Institute of Integrative Medicine, Department of Integrated Traditional Chinese and Western Medicine, Xiangya Hospital, Central South University, Changsha 410008, China
[f] School of Chemistry and Chemical Engineering, Center on Nanoenergy Research, Guangxi University, Nanning 530004, China
[g] Institute for Stem Cell and Regeneration, Chinese Academy of Sciences, Beijing 100101, China
[h] Department of Neurosurgery, Peking University Third Hospital, Beijing 100191, China

ARTICLE INFO

Article history:
Received 19 January 2022
Received in revised form 23 February 2022
Accepted 28 March 2022
Available online 3 April 2022

Keywords:
Nanogenerators
Low-level vagus nerve stimulation
Closed-loop control
Atrial fibrillation
Self-power
Implantable electronics

ABSTRACT

Atrial fibrillation is an "invisible killer" of human health. It often induces high-risk diseases, such as myocardial infarction, stroke, and heart failure. Fortunately, atrial fibrillation can be diagnosed and treated early. Low-level vagus nerve stimulation (LL-VNS) is a promising therapeutic method for atrial fibrillation. However, some fundamental challenges still need to be overcome in terms of flexibility, miniaturization, and long-term service of bioelectric stimulation devices. Here, we designed a closed-loop self-powered LL-VNS system that can monitor the patient's pulse wave status in real time and conduct stimulation impulses automatically during the development of atrial fibrillation. The implant is a hybrid nanogenerator (H-NG), which is flexible, light weight, and simple, even without electronic circuits, components, and batteries. The maximum output of the H-NG was 14.8 V and 17.8 μA (peak to peak). In the *in vivo* effect verification study, the atrial fibrillation duration significantly decreased by 90% after LL-VNS therapy, and myocardial fibrosis and atrial connexin levels were effectively improved. Notably, the anti-inflammatory effect triggered by mediating the NF-κB and AP-1 pathways in our therapeutic system is observed. Overall, this implantable bioelectronic device is expected to be used for self-powerability, intelligentization, portability for management, and therapy of chronic diseases.

© 2022 Science China Press. Published by Elsevier B.V. and Science China Press. All rights reserved.

1. Introduction

Atrial fibrillation (AF) is a prevalent cardiovascular condition with one of the highest rates of morbidity and death worldwide [1]. In the Global Burden of Disease project, an estimated 46.3 million individuals suffer from AF, with the number expected to rise by at least 72 million in Asia by 2050 [2]. The mechanism of AF reveals that the interaction between AF and the remodeling of the autonomic nervous system constitutes a vicious circle and exacerbates the condition rapidly [3]. A number of studies have applied low-level vagus nerve stimulation (LL-VNS) to inhibit AF inducibility. Electrical stimulation of the vagus nerve without reducing sinus heart rate or atrioventricular conduction is known as LL-VNS. LL-VNS is a promising therapeutic method for AF that can suppress autonomic nervous system remodeling to prevent a vicious circle [4]. In clinical trials the AF treatment outcomes of LL-VNS have been exciting [5]. In addition, LL-VNS can be applied to avoid the unfavorable consequences of vagus nerve stimulation (VNS), such as bradycardia and cardiac collapse [6]. Because of its good safety and few side effects, LL-VNS has been extensively used in epilepsy [7], myocardial infarction [8], heart failure [9], and other disorders. However, some fundamental challenges remain in terms of flexibility, miniaturization, and long-term service of bioelectric stimulation devices. These issues also have an impact on the future use of LL-VNS.

* Corresponding authors.
E-mail addresses: yangjbysy@bjmu.edu.cn (J. Yang), fenghongqing@binn.cas.cn (H. Feng), mclxmgs@126.com (G. Mao), zli@binn.cas.cn (Z. Li).
[1] These authors contributed equally to this work.

https://doi.org/10.1016/j.scib.2022.04.002
2095-9273/© 2022 Science China Press. Published by Elsevier B.V. and Science China Press. All rights reserved.

Zhonglin Wang and his colleagues [10] proposed triboelectric nanogenerators (TENGs) in 2012, which can transform microscopic mechanical energy into electricity in the environment. Since then, triboelectric nanogenerators and their applications have been extensively employed in power generation, biomedicine, artificial intelligence, and other fields [11–17]. Nanogenerators (NGs) have shown distinct benefits when used in implantable devices: They can gather mechanical energy both within and outside the human body and convert it to electricity, which eliminates the need for frequent battery replacements in implanted devices [18,19]. In addition, NGs have the characteristics of high flexibility and miniature size, ensuring the biocompatibility of implanted medical devices [20–23]. In recent years, NGs and related devices have been widely used to stimulate nerve [24,25]. These studies illustrate the advantages of NGs as an implantable neurostimulator.

In prior research, the majority of neurostimulators were performed without real-time monitoring of the patient's physical status [26]. This type of open-loop neurostimulation is potentially unable to achieve the intended goal and cause complications. Furthermore, continuous parasympathetic nerve stimulation has been linked to the development of fever, hoarseness, dyspnea, and cough [27]. Many studies have been conducted on the effects of closed-loop neurostimulation in an effort to treat epilepsy [28], pathological tremors [29], and overactive bladder [30]. It improved the effect of the experiment compared to the ordinary stimulus. The closed-loop neurostimulation system based on nanogenerator can be applied to LL-VNS to further improve the therapeutic effect for AF.

In this study, we designed a closed-loop self-powered LL-VNS system based on a hybrid nanogenerator (H-NG) for the routine treatment of patients with AF and tested its stability and biocompatibility. Then, the output range of the threshold that would influence heart rate (HR) was determined, and the effects of LL-VNS based on H-NG were experimentally verified on rats. These findings suggest that H-NG decreased AF duration and relieved the AF symptoms. Notably, an anti-inflammatory effect of LL-VNS mediated by the NF-κB and AP-1 pathways was observed. In addition, the output of the H-NG in the range of 5–15 μA (peak to peak) was beneficial for the treatment. Overall, this system with the advantages of self-powerability and intelligentization can bring in new insights for the therapy of chronic diseases.

2. Experimental

2.1. Materials

Polydimethylsiloxane (PDMS, Sylgard 184) was purchased from Dow Corning (USA). Polyvinylidene fluoride (PVDF) was purchased from Measurement Specialties, Inc. (USA), and TE Connectivity Company (China). Si-Pu (PMMA glue, acrylate, and methacrylate copolymer) was obtained from Beijing Solaibao Technology Co., Ltd. (China).

2.2. Fabrication of H-NG

A commercial metallized piezo film sheet was used as the piezoelectric material. The polarized PVDF membrane was coated with silver electrodes on both sides. First, the piezoelectric film was cut to specifications (2 cm × 5 cm) and sandpaper was used to rub and shear the edges to prevent short circuits. A thin polyimide (PI) film (300 μm) was pasted onto the lower surface of the polarized PVDF membrane to provide support. In contrast, we selected a polyethylene terephthalate (PET) film (2 cm × 5 cm, 1.5 mm) and paste-polarized PTFE film on its edge as a triboelectric layer. After that, the PVDF film with PI was placed in the mold, PMMA glue (acrylate and methacrylate copolymer) was added and covered to 3/5 (2 cm × 3 cm). Then, the PET film with the polarized PTFE film was gently covered on the PMMA glue. After incubation in an oven at 50 °C for 24 h, the PI film was covered on the surface of the device. The PDMS (Dow Corning, Sylgard 184) was poured into the mold with the device. All parts were attached layer by layer.

2.3. Component of the closed-loop LL-VNS system

A bracelet PENG sensor was reported in Ref. [31]. Bluetooth transmission module and micro-motor were purchased from LUILEC Technology Co., Ltd. (China). The full details are provided in Video S1 (online).

2.4. Characterization of H-NG

The mechanical properties of the H-NG were tested using a force gauge (Mark-10 ESM303, Mark-10 corporation, USA). The signals of the H-NG were measured using an electrometer (Keithley 6517 B, Tektronix, Inc., USA) and an oscilloscope (LeCroy HDO6104, Testwall Ltd., UK). A linear motor (LinMot E1100, LinMot Inc., USA) was used to provide the periodic external force applied to the H-NG (frequency of 2 Hz, operating distance of 30 mm, acceleration of 10 m/s^2, deceleration of 10 m/s^2, maximum speed of 10 m/s).

2.5. Animals and diets

All animal experiments were conducted under a protocol approved by the Committee on Ethics of the Beijing Institute of Nanoenergy and Nanosystems (A-2020016). Six- and eight-week-old male Sprague-Dawley rats were obtained from the Charles River (China). All rats were housed in separate cages with a 12-h light/dark cycle with free access to water and rodent chow Charles River (China). A week after adaptation, rats were randomly assigned to four groups (Multiple control groups are the primary means of eliminating confounding factors): control group (no surgery, no modeling and no treatment, n = 3), sham group (only surgery, n = 3), model group (AF modeling only, n = 3), and treatment groups (surgery + AF + LL-VNS, n = 9). Because the threshold of VNS is 30 μA, the stimulus strengths were 5 μA (n = 3), 10 μA (n = 3), and 15 μA (n = 3). Rats in the AF and AF + LL-VNS groups received a daily injection of 1 mL/kg acetylcholine (ACh)-$CaCl_2$ (66 μg/mL ACh and 10 mg/mL $CaCl_2$) in the tail vein for 7 d [32,33]. The AF + LL-VNS groups were treated with LL-VNS for 1 h after the fourth day. The sham groups were treated with bilateral vagus trunk electrode implantation, but no electrical stimulation experiment was performed. Rats in the control group received a daily injection of 1 mL/kg saline solution.

2.6. Surgical preparation

SD rats (male, 6–8 weeks, 200–250 g) were anesthetized with 1% pentobarbital sodium (30 mg/kg body weight) via intraperitoneal injection. The anesthetized mouse was placed in a supine position, and their limbs were held in place with medical tape. Hair clippers are used to shave the fur from the neckline to the mid-chest level. An incision of 2 cm was made on the median line of the cervix with the caudal terminus at the level of the clavicle. The sternohyoid and sternocleidomastoid muscles were bluntly separated with tweezers until the carotid sheath was exposed. After the carotid sheath was incised sharply, the vagus nerve was carefully dissociated with pointed tweezers placing a black suture underneath.

2.7. Measurement of cardiac electrophysiological signals

The vagus nerve threshold was measured in SD rats (male, 6–8 weeks, 200–250 g) (n = 3). For this purpose, the H-NG stimulated the vagus nerve at different current intensities. The HR change rate was observed after 60 s of stimulation. HR recovery was observed after cessation of stimulation. The electrocardiogram (ECG) 100C module of a physiological signal recording system (MP150WSW, BIOPAC, USA) was used to measure the whole process and calculate the heart rate variability (HRV). The ECG of rats in all groups was recorded using a physiological signal apparatus. Origin 8.0 was used for analysis. The full details are provided in Video S2 (online).

2.8. H&E and Masson staining of atrial tissue

The hearts of rats were promptly removed under anesthesia, fixed with 10% neutral formalin fixative, embedded in paraffin, and sectioned. Microscopy was performed using an HE staining kit (Solarbio, G1120), neutral gum sealing, and a panoramic scanner (3DHISTECH P250 FLASH, 3DHISTECH Ltd., USA). After staining with an improved Masson tri-color solution (Solarbio, G12345), neutral gum was sealed, and a panoramic scanner was used to observe the results. Image-Pro 6.0 was used to evaluate the results.

2.9. Immunohistochemistry of atrial tissue

After typical paraffin sectioning, the slides were treated overnight at 4 °C with Rabbit Polyclonal anti-CX43/GJA1 antibody (Abcam, AB11370, diluted to 1:2000), anti-Bax polyclonal antibody (Solarbio, K001593P, diluted to 1:100), and anti-Bcl-2 polyclonal antibody (Solarbio, K001594P, diluted to 1:100). The samples were evaluated using a panoramic scanner (3DHISTECH P250 FLASH, 3DHISTECH Ltd.), and each sample was studied in three random fields. Image-Pro 6.0 was used to evaluate the results.

2.10. H-NG biocompatibility in vivo

After surgical suturing, the H-NG was implanted subcutaneously. The morphology and position of the H-NG were measured using micro-CT and 3D reconstruction for four weeks. Histological evaluation of the *in vivo* biocompatibility was performed. The skin tissue, liver, kidney, spleen, lung, and heart around the skin slice were rapidly removed under anesthesia four weeks after implantation. The cells were examined using a panoramic scanner (3DHISTECH P250 FLASH, 3DHISTECH Ltd.) after staining with H&E (Solarbio, G1120). The performance of the H-NG implanted is shown in Video S3 (online).

2.11. Serum concentrations of TNF-α and IL-6

The 3 mL arterial blood was taken from the abdominal aorta and centrifuged for 10 min at 4 °C and 8000 *g*. The supernatant was collected, and TNF-α and IL-6 levels were determined using an ELISA kit (Solarbio, SEKR-0005, SEKR-0009).

2.12. Statistical analysis

The statistical significance of the differences was determined using one-way ANOVA analysis of variance. Data were analyzed as mean ± standard error of mean (SEM) in GraphPad Prism v. 6 (GraphPad Software Inc., USA). Differences were considered statistically significant at $P < 0.05$, $P < 0.01$, and $P < 0.001$ were considered statistically significant and were labeled with *, **, ***, and *ns*, respectively; $^*P < 0.05$, was considered statistically significant.

3. Result and discussion

3.1. System design

We designed a closed-loop self-powered LL-VNS system based on triboelectric nanogeneration technology. The system was divided into three modules: sensing, signal processing, and therapy (Fig. 1a). The sensing module consisted of a PENG sensor, a wristband, and a Bluetooth module. The PENG sensor extracted pulse waves from the skin and transmitted data through a Bluetooth module. The signal processing module was mostly dependent on mobile phones and applications. It monitored the occurrence of AF by analyzing the pulse waveform to alert the patient in real time (Fig. S1a, b online). When AF occurs, the wristband sends out a timely warning message. Users can tap this device to exert its anticholinergic effect by suppressing the activity of the vagus nerve, so as to prevent atrial fibrillation inducibility to achieve therapeutic effects. At the same time, the users can see their pulse waves on their phones and monitor their health in real time (Fig. S1c online). Fig. 1c shows a circuit diagram of the system.

The treatment module consists of two components: an H-NG stimulator and the hands. The H-NG stimulator was an important component of the closed-loop LL-VNS system. It was mainly composed of triboelectric, piezoelectric, and encapsulation modules. Piezoelectric and triboelectric modules were the core components of the H-NG, which converted external mechanical energy into electrical energy. The piezoelectric material was polarized PVDF, and its surface was covered with two Ag electrode layers. For the triboelectric module, the Ag electrode and polarized PTFE were used as two triboelectric layer materials. Additionally, Si-PU was used as a spacer and was half-filled. This design effectively reduced the impact of miscontact on the H-NG and significantly increased the stability of the system. The entire device was packaged with thin PDMS to ensure performance and prevent the device from being invaded by the liquid environment.

3.2. Principle and characterization of H-NG

Safety and durability are the most important features of implantable electronic devices for neurostimulation [34]. To fit the daily treatment characteristics of patients with AF, we designed an H-NG device as an energy source. In order to more efficiently harvest the mechanical energy generated at a particular location, we designed a hybrid structure for separating half of triboelectric layer and piezoelectric layer. This "switch" design provides a spacer for the triboelectric module. Besides, it reduces the risk of additional stimulation caused by accidental contact with the device, which can greatly improve the device security and system stability.

The working process of the H-NG is illustrated in Fig. 2a. In the initial state, the top layer was separated from the bottom layer, and there was no triboelectric or piezoelectric potential between the different electrodes. When force was applied to the device, the right side of the device deformed and brought the upper and bottom triboelectric layers together. In this process, with the increase in stress, the contact surface of the upper and lower triboelectric layers gradually increased. Then, the stress on the piezoelectric material adhering to the lower surface gradually increased. When the top layer was fully in contact with the bottom layer, the piezoelectric and triboelectric potentials both reached a maximum. If these different electrodes were connected by an external circuit, the current would appear during the deformation process of the H-NG. When the force was released, the upper and lower layers were restored to their original state, and the electrons were driven back to the upper layer by piezoelectric and triboelectric poten-

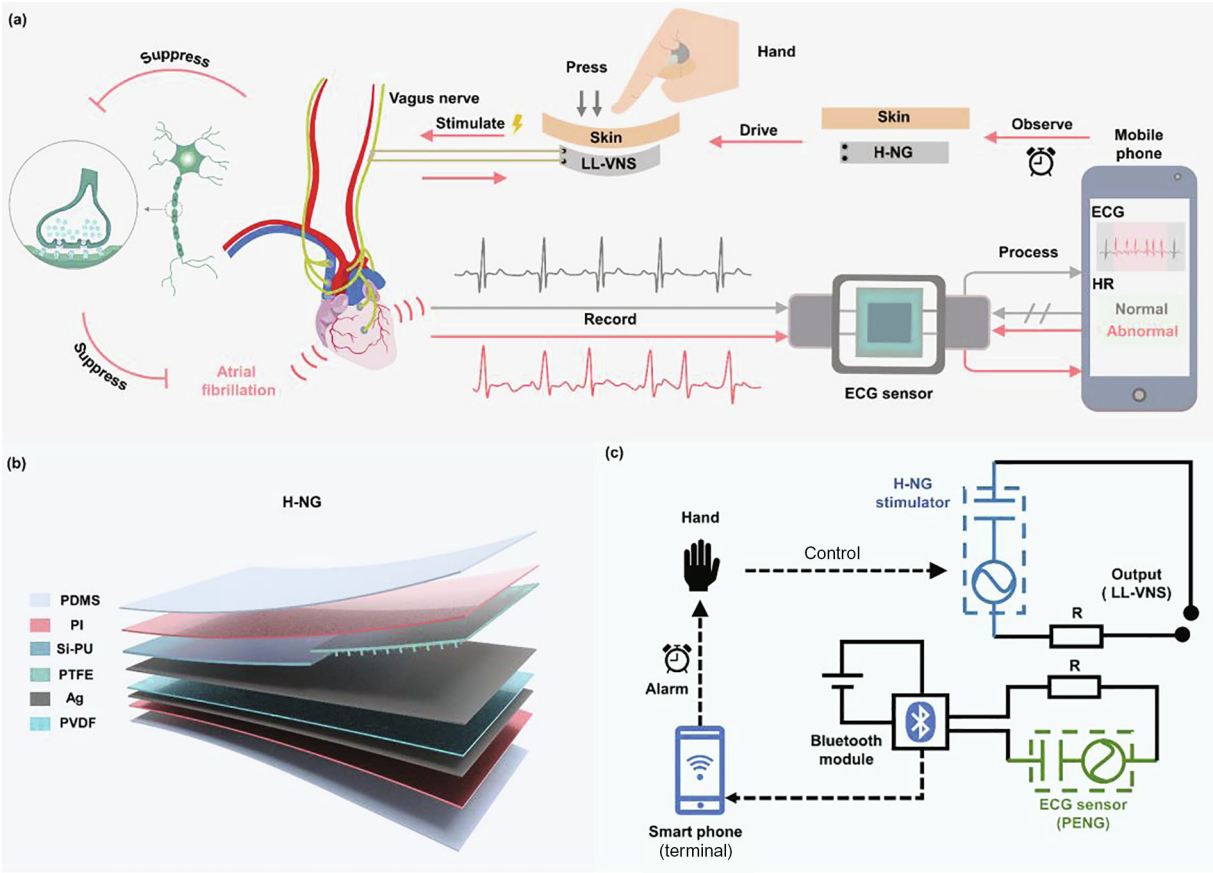

Fig. 1. Overview and principle of the H-NG based closed-loop self-powered LL-VNS system. (a) Illustration of the H-NG based closed-loop self-powered LL-VNS system. (b) Structure of H-NG. (c) Circuit diagram of H-NG based closed-loop LL-VNS system.

tials. Fig. 2b shows the output difference between the H-NG and the pure piezoelectric device without the triboelectric module.

To demonstrate the working performance of the H-NG, we characterized the short-circuit current, open-circuit voltage, and instantaneous power at different impedances. As shown in the Fig. 2c and Fig. S2a–c (online), the maximum current and voltage of H-NG were 17.8 μA (peak to peak) and 16.7 V, respectively. Meanwhile, with the increase in impedance, the maximum instantaneous was 35 μW at 2.3 MΩ (Fig. 2d). After using the triboelectric module, the voltage of the device increased by 110% and the current increased by 210%. The results show that the "switch" structure can greatly improve the electron transfer efficiency.

The mechanical response of the device was also one of the properties we considered [35–37]. Linear motors were used to simulate the forces within the human range. As shown in Fig. 2e, the H-NG had excellent linearity of current and applied force, which also proves its maneuverability. Fig. 2f shows the working performance of the device at different frequencies. Because the operating frequency must be consistent with the hand movement frequency, we choose 1–3 Hz for frequency testing. It can be seen that as the frequency gradually increased, the current did not increase significantly. Finally, 10,000 s working tests were carried out to verify the working durability of the device. Fig. 2g shows that the performance of the device hardly decreased during the testing cycle.

3.3. Biocompatibility of the H-NG in vivo

Excellent biocompatibility is required to avoid undesirable biological responses [38–40]. The use of PDMS as the encapsulation layer in the device can significantly improve the flexibility and sealing of the H-NG. Meanwhile, in order to explore the biocompatibility of the device, the sealed H-NG was implanted subcutaneously in the rear of the rat for four weeks (Fig. 3a and Fig. S3a–e online), and the H&E staining of rats was observed (Fig. 3b). Histological sections of the skin showed no substantial inflammatory response, and a number of cicatrices were observed. Meanwhile, there was no injury to the visceral organs. The performance of the H-NG implanted showed that the human tap could produce a 5–15 μA current. This is consistent with the device output required for the AF therapy (Fig. 3c). The micro-CT scans displayed the H-NG transverse, sagittal, and coronal planes, and no breakage or significant movement of the device was observed (Fig. 3d). H-NG has excellent sealing properties and an unchangeable position *in vivo*, which ensures accuracy and stability when the external force drives the internal device. During 3D reconstruction in CT, the H-NG was found below the ribs and on the right side of the spine (Fig. 3e). The respiration, heartbeat, and routine activity of the rat were unaffected by this placement. The results demonstrate that H-NG has outstanding biocompatibility and output stability.

3.4. Measurement of electrical stimulus strength for LL-VNS

In previous reports, the definition of LL-VNS in rats was unclear [41–43]. In this work, the threshold for the vagus nerve was the electrical stimulus strength that can greatly change the HR within dozens of seconds. LL-VNS was defined as less than half of the vagus nerve threshold. The influence of stimulus strength on HR change rate contributes to the detection of the vagus electrical stimulation threshold of the H-NG. In the experiment, we found

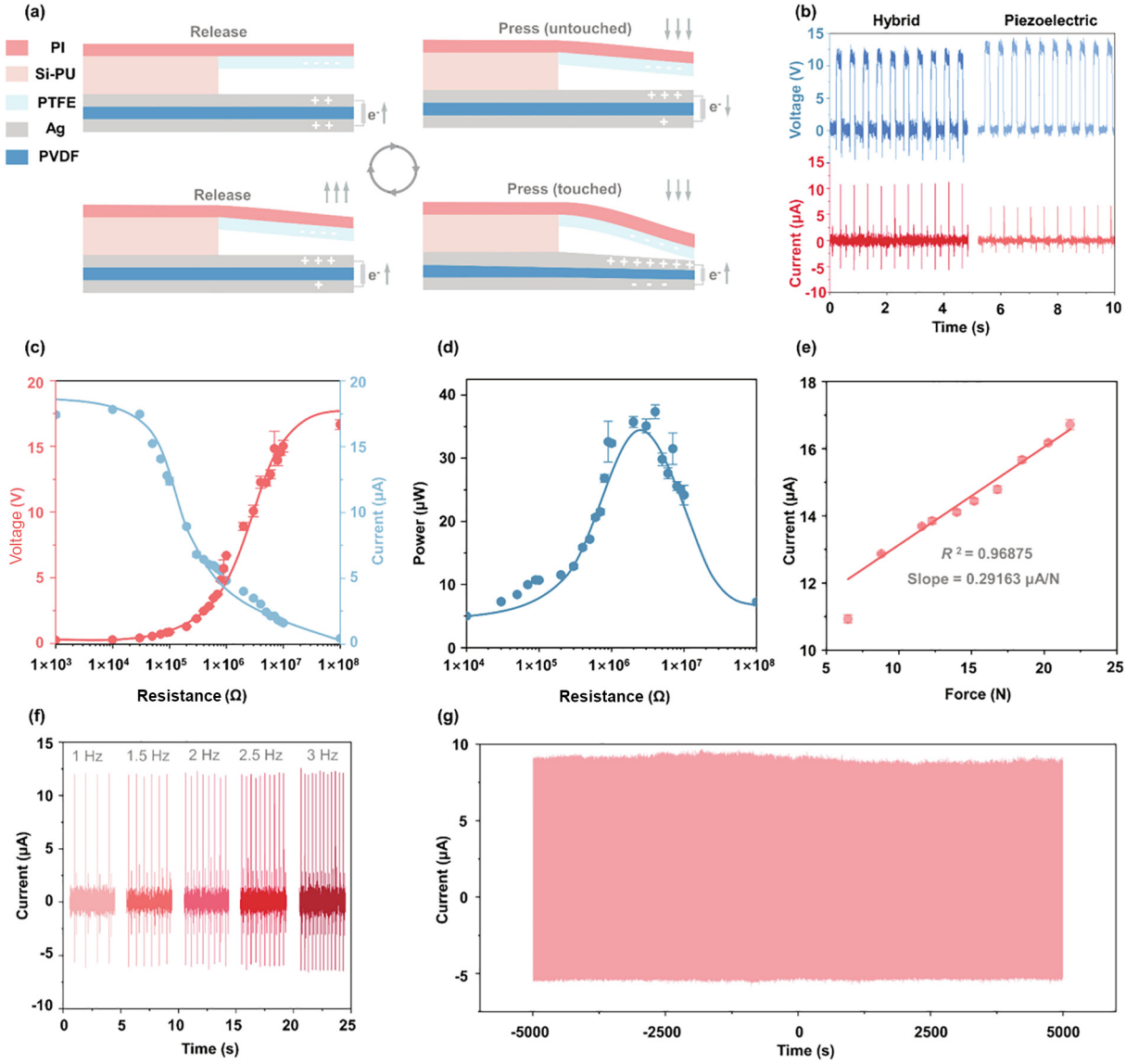

Fig. 2. Characterization of the H-NG. (a) The working principle of H-NG. (b) The difference between the performance of Hybrid-NG and the piezoelectric module. (c) The variation of voltage and current. (d) Power of the H-NG with different external load resistance. (e) Overall linearity of the applied force and the output current of the H-NG. (f) Current of H-NG with different frequency. (g) Stability test of the H-NG under continuous operation for 10,000 s.

that when the intensity of stimulation was 80–300 μA, the range of HR changed by more than 40% (Fig. S4 online). When the stimulus strength was 300 μA, the thresholds of the three nerve fibers A, B, and C reached at the same time, and the heart rate dropped most obviously at this time. The HR change rate gradually decreased when the stimulus strength was less than 80 μA (Fig. 4a). When the stimulation was interrupted, the vagus nerve was no longer excited and the release of acetylcholine stopped. Meanwhile, acetylcholinesterase worked to degrade acetylcholine. The downward trend was obvious during 60 s of stimulation, and the HR gradually increased. Based on this result, we mainly explored the effect on rats of stimulation with a current intensity below 80 μA. When the current intensity was below 30 μA, the amplitude of the HR change was less than 5%. There was no difference in HR between the stimulus strengths of 30 and 20 μA (Fig. 4b). These results suggest that 30 μA may be the threshold for vagus nerve stimulation.

HRV is also an important parameter for exploring the vagus nerve stimulation threshold. It refers to the balance in the autonomic nervous system, which is related to the excitability of the sympathovagal nerve. When the vagus nerve is given suprathreshold stimulation, the excitability of the vagus nerve increases and HRV decreases. When subthreshold stimulation of the vagus nerve is given, the excitability of the vagus nerve and the sympathetic nerve is kept in balance, and the HRV remains at a normal level. High frequency (HF) and low frequency (LF) represent the high- and low-frequency domains in the electrocardiogram, respectively. The ratio of LF to HF represents HRV. In the gradient range from 40 to 70 μA, HRV decreased with increasing current intensity, indicating that vagus nerve excitability gradually increased. However, at 30 μA, HRV returned to normal (Fig. 4c). There was no difference in the effect of 30 and 20 μA on HRV. Other experimental groups also obtained the same conclusion (n = 3), which proved that the threshold of VNS in rats was 30 μA. Therefore, we chose stimulus strength of 5–15 μA as the LL-VNS.

3.5. LL-VNS reduce AF duration in rat AF models

To test the effect of LL-VNS on rats with AF, we established a rat model of AF and demonstrated the stability of the model through

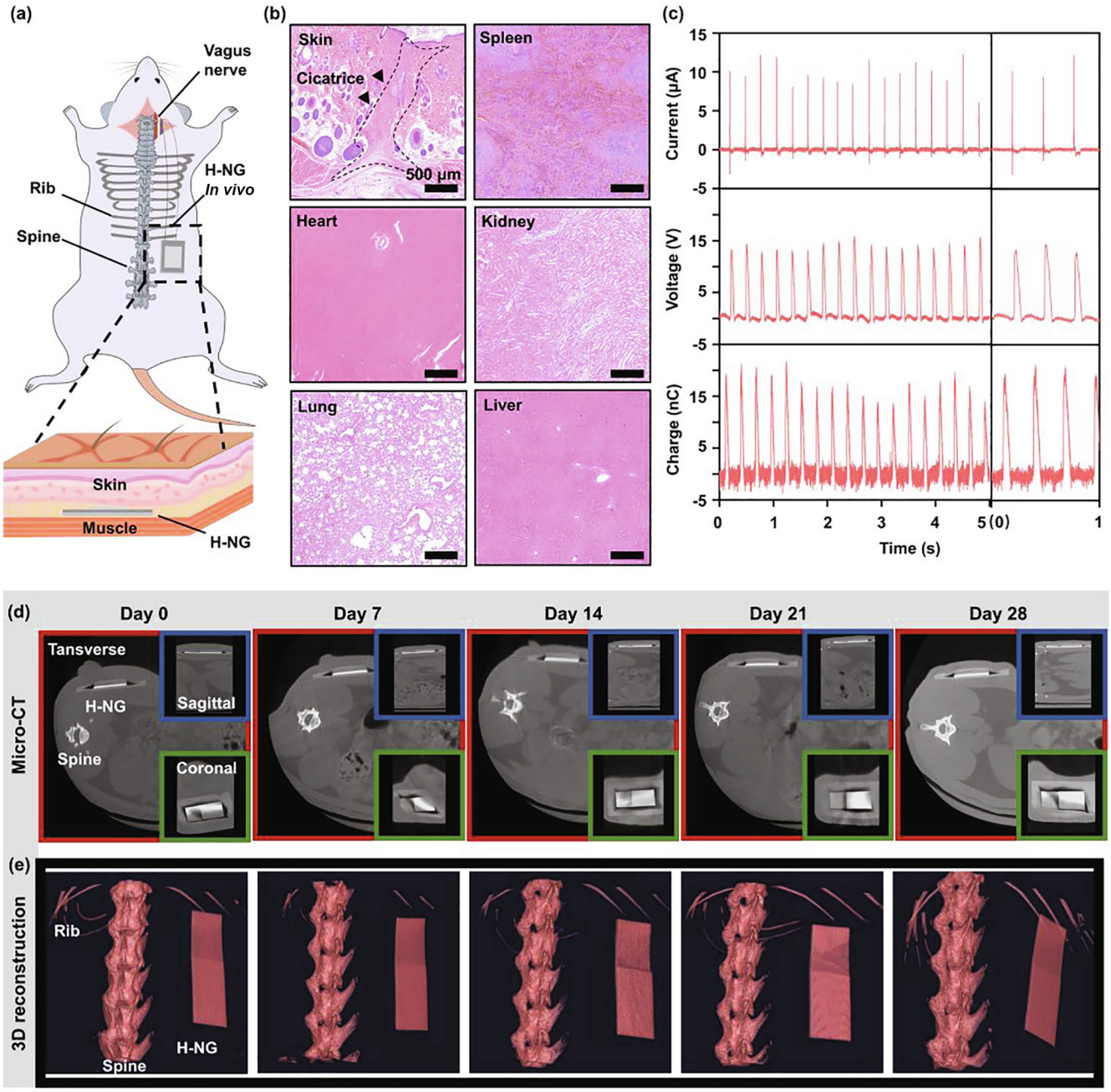

Fig. 3. Biocompatibility of the H-NG *in vivo*. (a) The illustration of a rat implanted with the H-NG subcutaneously. (b) H&E staining of the rat skin, spleen, liver, heart, kidney, lung implanted with the H-NG subcutaneously after 4 weeks. (c) The performance of H-NG implanted. (d) Micro-CT image of a rat implanted with the H-NG subcutaneously for 4 weeks. (e) 3D reconstruction image of the H-NG implanted into the rat subcutaneously for 4 weeks.

multi-group experiments (Fig. S5 online). In the experiment, the experimental group received injections of the drug over seven days and electrical stimulation starting on the fourth day. The model group was only injected with the drug without stimulation. The experiment reveals that LL-VNS does not change the HR over time, indicating that the device output is stable, and the experimental results are legitimate (Fig. S6a–c online). Four seconds after the drug injection, the ECG indicated an obvious AF waveform, which was characterized by the absence of P waves and the substitution of F waves, as well as an unequal R-R interval and R wave voltage. AF duration is defined as the interval from the emergence of AF waves to the return of normal sinus rhythm. The AF duration increased dramatically in the model group, indicating that the cardiac injury was gradually aggravated (Fig. 4d and Fig. S7a online). In contrast, after the fourth day of LL-VNS, AF duration was reduced in the LL-VNS+AF group (Fig. 4e and Fig. S7b online). This proves that LL-VNS can effectively reduce the duration of AF. However, because the heart muscle was already damaged, the duration of the treatment group was no less than that of the first day. At the same time, we found wide and distorted abnormal QRS waves in the experiment, which may indicate premature ventricular contraction. Premature ventricular contractions are prodromal signs of AF, indicating abnormal electrical conduction in atrial myocytes [44]. On the first four days, the AF durations of the experimental and model groups increased simultaneously (Fig. 4f). On the last four days, the AF duration in the experimental group began to

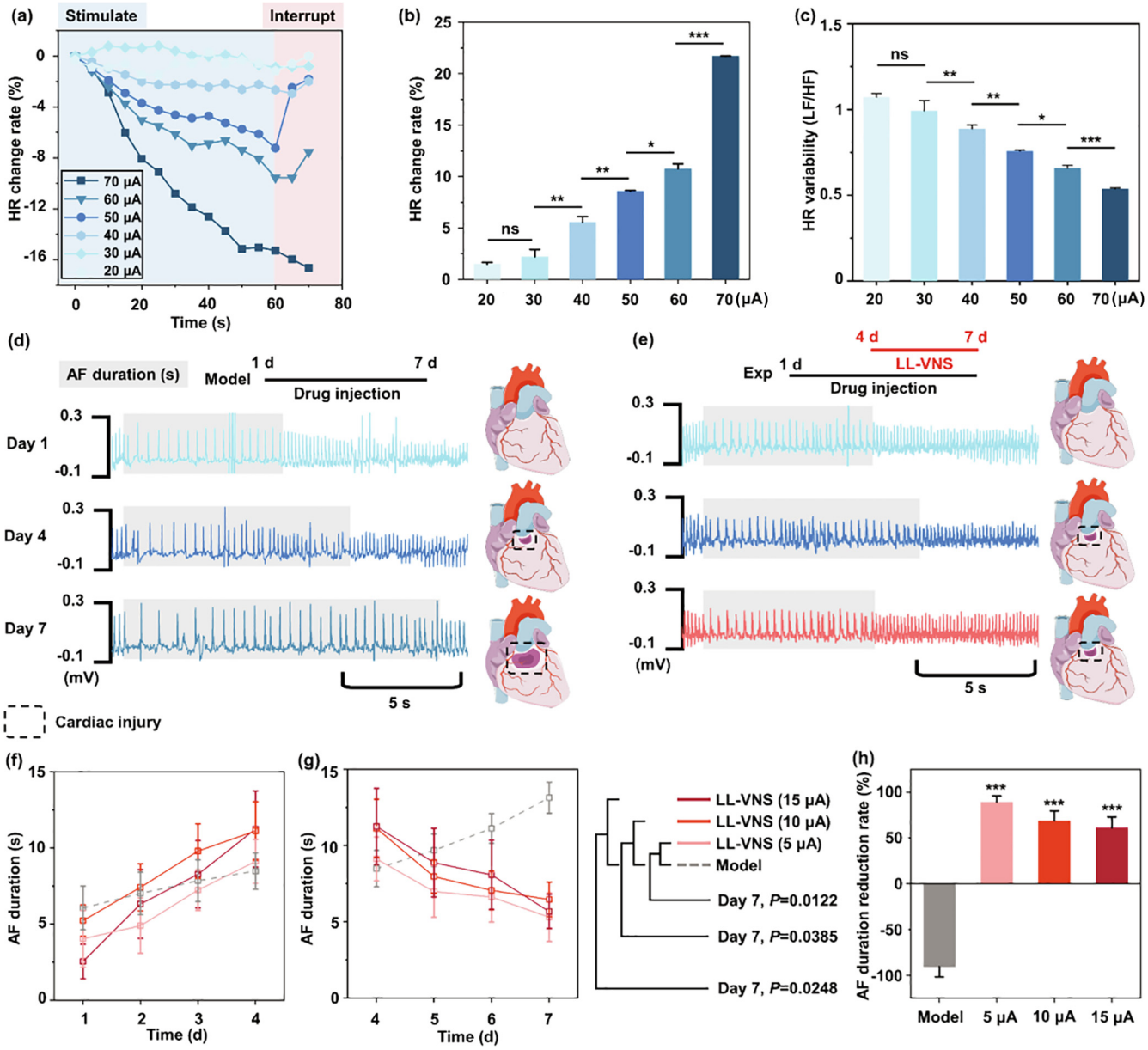

Fig. 4. ECG characterization of rats. (a) HR change rate stimulated by different stimulus strength from 20 to 70 μA for 60 s. (b) HR change rate at different stimulus strength (n = 3). (c) HR variability at different stimulus strength (n = 3). (d) AF duration in the model group for 7 days continuous drug injection. (e) AF duration in the experimental group treated with LL-VNS after the fourth day. (f) Comparison of AF duration between the model group and experimental group on the first four days (n = 3). (g) Comparison of AF duration between the model group and experimental group on the last four days (n = 3). (h) Comparison of AF duration reduction rate between the model group and experimental group.

decrease (Fig. 4g). AF duration reduction rate refers to the ratio of the change in the AF duration in the last four days to the change in the AF duration in the first four days. After statistical analysis, the AF duration significantly decreased by 60%–90% after LL-VNS therapy (Fig. 4h). Notably, different rats have varying levels of medication tolerance, and AF duration still shows great differences among the groups. In conclusion, LL-VNS can successfully minimize AF duration to relieve cardiac injury, and a stimulus strength of 5–15 μA has a good effect.

3.6. LL-VNS alleviated the pathological changes of rat AF models

AF causes myocardial cell apoptosis and inflammatory infiltration of atrial tissue. The overburdened normal atrial muscle becomes hypertrophic or overstretched as a result of atrial muscle apoptosis. Abnormal collagen fibers are deposited in the interstitium of atrial myocytes. The autonomic nervous system underwent remodeling to cater to changes in the atria (Fig. 5a). H&E staining is a critical pathological examination for detecting myocardial morphological injuries. Myocardial cells were dyed pink, and inflammatory cells were dyed blue-purple in H&E staining. The arrangement of myocardial cells in the control and sham groups was orderly and dense, and the morphology of the myocardial tracts was complete. The model group showed abundant fibrous connective tissue, extensive infiltration of inflammatory cells, and a small amount of hemosiderin deposition (black dotted area). Fibrous connective tissue can be found as an irregular, loose grid. Muscle fibers are broken and loose with wide gaps. However, there was only a small amount of fibrous connective tissue and inflammatory cell infiltration in the LL-VNS+AF group. In summary, AF

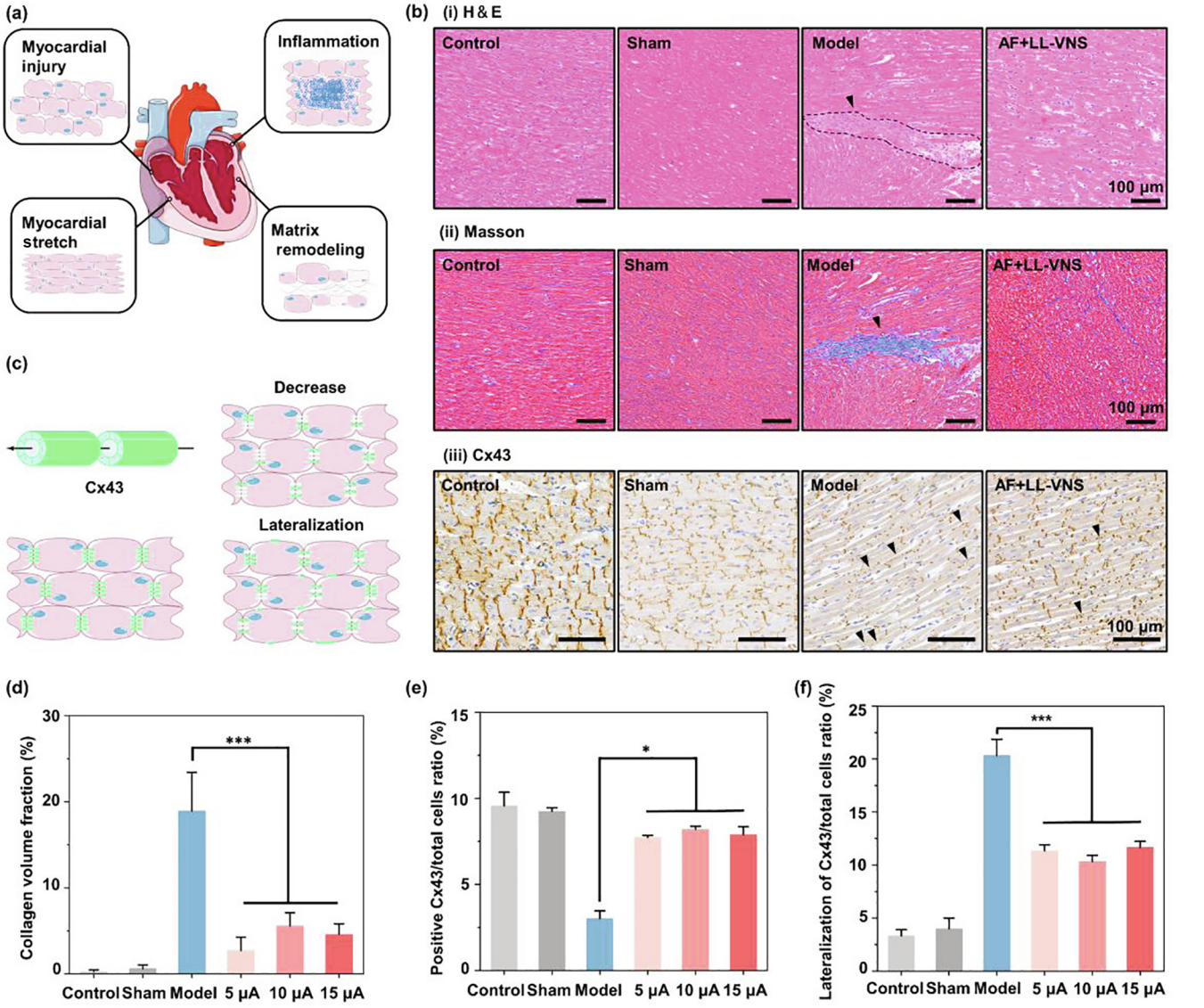

Fig. 5. Pathological feature of rats. (a) Schematic diagram of cardiac pathological changes after AF. (b) Cardiac pathological changes after AF. (i) Myocardial morphological injury (H&E staining, $n = 3$). (ii) Myocardial fibrosis (Masson staining, $n = 3$). (iii) Atrial connexin levels (Immunohistochemistry staining, $n = 3$). (c) Schematic diagram of Cx43 changes after AF. (d) Myocardial fibrosis treated with LL-VNS. (e) Change in the number of Cx43 treated with LL-VNS. (f) Change in Cx43 distribution treated with LL-VNS, particularly lateralization of Cx43.

modeling resulted in significant pathological changes (Fig. 5b(i) and Fig. S8a online).

In Masson staining, myocardial cells were stained red and collagen fibers were stained blue. The myocardium in the model group was severely disordered and loose, and the myocardial space widened. The myocardial tracts were surrounded by a large grid of blue fibrous connective tissue, with this large area replacing the normal myocardium (Fig. 5b(ii) and Fig. S8b online). After LL-VNS treatment, the collagen volume fraction (CVF) was markedly lower than that in the model group (blue) (Fig. 5d). In the VNS +AF group (red), CVF was the lowest at 5–15 μA, indicating that the 5–15 μA group had a good effect on improving myocardial fibrosis.

To determine changes in atrial connexin levels after AF, connexin 43 (Cx43) levels were measured using immunohistochemistry. Studies have shown that Cx43 contains six connexins arranged in a circle, and connexins within cells connect with connexins within adjacent cells through gap junctions to form electrical conduction between atrial myocytes (Fig. 5c). AF is an abnormal electrical conduction activity of the myocardium, which means that AF may be associated with changes in the number and distribution of atrial connexins [45]. A decrease in atrial connexin and an increase in lateralization were the most common symptoms of AF (Fig. 5b(iii) and Fig. S8c online). Compared with the control group, the expression of Cx43 in the model group was significantly reduced, and the lateralization of Cx43 was enhanced. A comparison between the LL-VNS+AF group and the model group showed that LL-VNS improved Cx43 expression and weakened the lateralization of Cx43 (Fig. 5e, f). Atrial myocyte apoptosis is one of the main pathological changes in AF. By preventing the apoptotic process, the loss of atrial myocytes and cardiac damage produced by AF can be avoided [46,47]. In this study, LL-VNS upregulated the expression of Bcl-2 protein and downregulated the expression of Bax protein in atrial myocytes, thereby inhibiting the apoptosis of atrial myocytes (Fig. S8d, e online). In summary, LL-VNS could dramatically improve the changes in atrial connexin induced by AF, and the stimulus strength of the 5–15 μA group was significantly effective.

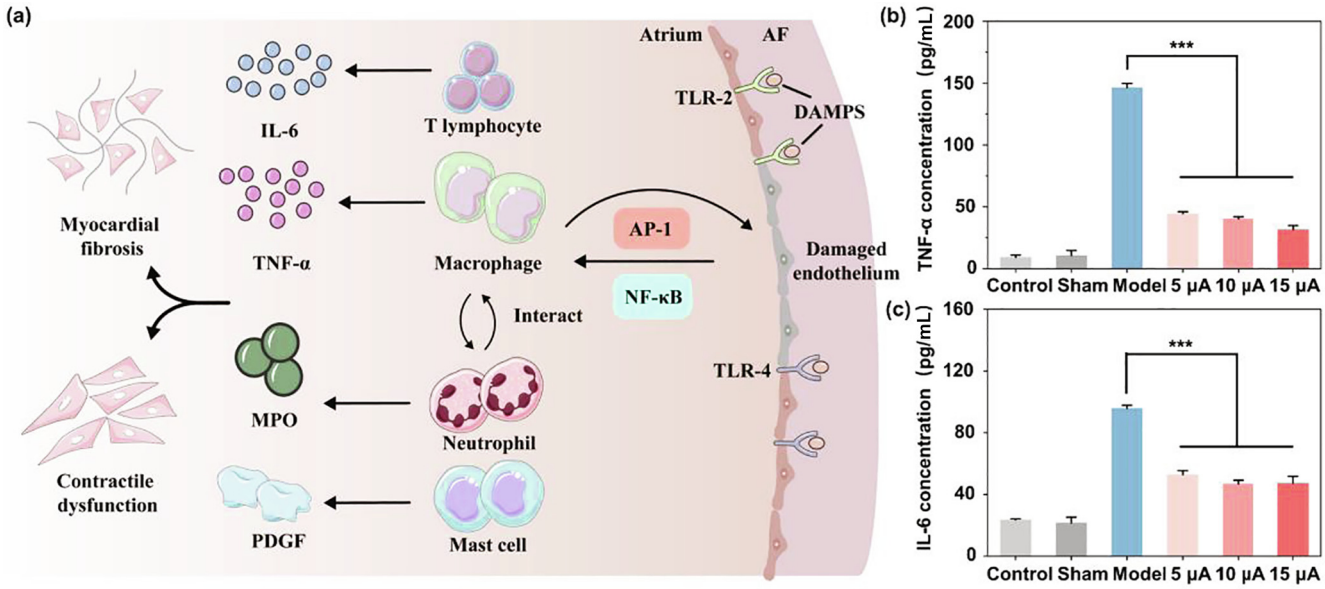

Fig. 6. Anti-inflammatory effect of the H-NG. (a) Schematic diagram of inflammatory cell regulation in AF. (b) TNF-α and (c) IL-6 concentration at different groups (Elisa kit, n = 3).

3.7. Anti-inflammatory effects of LL-VNS

It is well proved that the levels of Toll-like receptors (TLR-2 and TLR-4) are elevated in the atrium in patients with AF [48]. Inflammation in cardiac injury is triggered by the same inherent pattern recognition mechanisms that are employed to identify microbes. However, immunostimulatory molecular patterns in sterile inflammation are distinct from those seen in infectious inflammation and are canonically related with damage. Thus, they are called danger-associated molecular patterns (DAMPS). The release of DAMPS binds toll-like receptors on the cell surface to induce the expression of pro-inflammatory genes through the nuclear factor NF-κB and transcription factor AP-1 in a cell-specific manner, thereby activating innate and adaptive immune responses (Fig. 6a). In clinical studies, serum TNF-α level is higher in patients with AF than in those with sinus rhyth. Correspondingly, an increase in TNF-α will increase the degree of atrial fibrosis and atrial matrix remodeling. In addition, IL-6 is associated with blood hypercoagulability, platelet activation, and endothelial damage caused by AF. Meanwhile, neutrophils and mast cells are also activated, and substantial amounts of myeloperoxidase (MPO) and platelet-derived growth factors (PDGF) are released. MPO and PDGF stimulate fibroblasts, which results in increased collagen production and atrial fibrosis [49]. Despite the activation of separate inflammatory cascades, these processes may interact and coexist in patients with AF. As a result, low levels of TNF-α and IL-6 significantly reduced the risk factors associated with inflammation in AF. Atrial inflammation leads to myocardial injury and remodeling. A vicious cycle between atrial fibrillation and inflammation can aggravate pathological process of atrial fibrillation. The concentrations of TNF-α and IL-6 inflammatory factors in atrial within 24 h were measured using the ELISA kit. There was a low level of inflammation in the control and sham groups, but high in the model group. Compared with the model group, the inflammatory molecules in arterial blood decreased in the AF + LL-VNS group (Fig. 6b, c). The experimental results showed that LL-VNS could reduce the infiltration of inflammatory factors after AF and prevent further damage of inflammatory factors by myocardial cells.

4. Conclusion

We designed a closed-loop self-powered LL-VNS stimulation system based on the H-NG, which can be used for the daily care of patients with AF. The system monitored the wearer's pulse waves in real time through a wrist bracelet and identifies the onset of atrial fibrillation through a mobile phone. Consequently, the therapy module provides a force to power the H-NG stimulator. An output of 5–15 μA (peak to peak) can be generated using our device within the manual range. The closed-loop design of the device can effectively reduce the side effects of constant stimulation and improve the security and stability of the system. This work also innovatively used a specially constructed NG as a vagus nerve stimulator and demonstrated that the ultra-low intensity output produced by it can effectively treat AF. At the same time, we explored the optimal stimulus parameters and proved their reliability through a large number of biological experiments, which has guiding significance for further research.

Durability is also an important factor in a vagus nerve stimulation device. Most existing nerve stimulation devices use chips as controllers to generate electrical pulses [50]. These devices tend to have very stable outputs, but are usually not used for a long time owing to the capacity of the battery. With the development of nanogenerator technology, NG has been widely used in nerve stimulation due to its characteristics of low energy consumption and high biosafety. The H-NG used in this work can directly convert mechanical energy into electrical energy, eliminating the need for batteries, thus greatly increasing the service life of the device [51,52]. The H-NG can generate 5–15 μA (peak to peak) in the manual range, while LL-VNS in this range has been proven to be effective in animal experiments and other biological tests. Besides, the performance of H-NG shows good linearity in the range of 5–20 N. This further proves the reliability of the H-NG when applied to daily life. The system can also be optimized for automation and closed-loop control and closed-loop design can effectively improve the efficiency of treatment and improve the life quality of patients.

Antiarrhythmic is a good property for systems based on the H-NG. After the H-NG was used for neurostimulation, it greatly

reduced AF duration and improved the pathological changes in AF, which proves that it can balance the electrical conduction activities between cardiomyocytes. H-NG-based LL-VNS successfully breaks the vicious cycle of atrial remodeling after AF and has good antiarrhythmic properties. It is promising to inhibit ventricular fibrillation inducibility and alleviate the severity of ischemia–reperfusion injury after myocardial infarction.

LL-VNS is well known for its anti-inflammatory properties. Inflammation during AF can worsen symptoms, which demonstrates that the anti-inflammatory effects of implanted devices should be taken seriously. However, Table S1 (online) shows that few studies have focused on the anti-inflammatory effect of the implanted device used for vagus nerve stimulation after comparing other studies on the treatment of AF. In our experiment, H-NG was observed to have an excellent anti-inflammatory effect by using an extremely low current. This will bring treatment to more patients in the future due to the synergistic effect of inflammation in numerous diseases.

In summary, the closed-loop VNS system has been applied to diseases such as epilepsy and Parkinson's disease. LL-VNS has a far lower stimulus strength than VNS, which implies less influence on organs and fewer adverse effects. In our closed-loop system, when atrial fibrillation occurs, the patient can be reminded to treat themselves on demand in a timely manner. Meanwhile, the closed-loop LL-VNS based on nanogenerators has excellent antiarrhythmic and anti-inflammatory properties, which can greatly improve the targeting of stimulation therapy. In the future, the system can help to promote the in-home health monitoring and reduce the cost of clinical treatment.

Conflict of interest

The authors declare that they have no conflict of interest.

Acknowledgments

This work was supported by Beijing Natural Science Foundation (JQ20038), the Strategic Priority Research Program of the Chinese Academy of Sciences (XDA16021101), and the National Natural Science Foundation of China (T2125003, 61875015, and 81971770).

Author contributions

Yu Sun and Shengyu Chao designed and carried out most of the experiments and analyzed the data. Han Ouyang, Gengsheng Mao, and Zhou Li supervised and revised the experimental protocol. Weiyi Zhang contributed to material encapsulation. Weikang Luo and Qingbin Nie collaborated to help implement animal experiments. Jianing Wang, Changyi Luo, Gongang Ni, and Lingyu Zhang collaborated to analyze the data. Yu Sun and Shengyu Chao wrote the original draft. Hongqing Feng, Gengsheng Mao, and Zhou Li reviewed and revised the manuscript. All authors discussed the results and commented on the manuscript.

Appendix A. Supplementary materials

Supplementary materials to this article can be found online at https://doi.org/10.1016/j.scib.2022.04.002.

References

[1] Chung MK, Refaat M, Shen WK, et al. Atrial fibrillation: JACC council perspectives. J Am Coll Cardiol 2020;75:1689–713.
[2] Kornej J, Borschel CS, Benjamin EJ, et al. Epidemiology of atrial fibrillation in the 21st century: novel methods and new insights. Circ Res 2020;127:4–20.
[3] Hou Y, Zhou Q, Po SS. Neuromodulation for cardiac arrhythmia. Heart Rhythm 2016;13:584–92.
[4] Sheng X, Scherlag BJ, Yu L, et al. Prevention and reversal of atrial fibrillation inducibility and autonomic remodeling by low-level vagosympathetic nerve stimulation. J Am Coll Cardiol 2011;57:563–71.
[5] Stavrakis S, Stoner JA, Humphrey MB, et al. TREAT AF (transcutaneous electrical vagus nerve stimulation to suppress atrial fibrillation): a randomized clinical trial. JACC Clin Electrophysiol 2020;6:282–91.
[6] Capilupi MJ, Kerath SM, Becker LB. Vagus nerve stimulation and the cardiovascular system. Cold Spring Harb Perspect Med 2020;10:a034173.
[7] Qin X, Lin S, Yuan Y, et al. Vagus nerve stimulation for pediatric patients with drug-resistant epilepsy caused by genetic mutations: two cases. J Neurorestoratology 2020;8:138–48.
[8] Hamann JJ, Ruble SB, Stolen C, et al. Vagus nerve stimulation improves left ventricular function in a canine model of chronic heart failure. Eur J Heart Fail 2013;15:1319–26.
[9] Wang Z, Yu L, Wang S, et al. Chronic intermittent low-level transcutaneous electrical stimulation of auricular branch of vagus nerve improves left ventricular remodeling in conscious dogs with healed myocardial infarction. Circ Heart Fail 2014;7:1014–21.
[10] Fan FR, Tian ZQ, Wang ZL. Flexible triboelectric generator. Nano Energy 2012;1:328–34.
[11] Wang ZL. On the expanded Maxwell's equations for moving charged media system – general theory, mathematical solutions and applications in TENG. Mater Today 2021;20:74–82.
[12] Zhang Q, Jin T, Cai J, et al. Wearable triboelectric sensors enabled gait analysis and waist motion capture for IoT-based smart healthcare applications. Adv Sci 2021;9:2103694.
[13] Li D, Xu C, Liao YJ, et al. Interface inter-atomic electron-transition induced photon emission in contact-electrification. Sci Adv 2021;7:eabj0349.
[14] Chen L, Wen C, Zhang SL, et al. Artificial tactile peripheral nervous system supported by self-powered transducers. Nano Energy 2021;82:105680.
[15] Zhang N, Qin C, Feng T, et al. Non-contact cylindrical rotating triboelectric nanogenerator for harvesting kinetic energy from hydraulics. Nano Res 2020;13:1903–7.
[16] Zhao X, Askari H, Chen J. Nanogenerators for smart cities in the era of 5G and Internet of Things. Joule 2021;5:1391–431.
[17] Zhou Z, Chen K, Li X, et al. Sign-to-speech translation using machine-learning-assisted stretchable sensor arrays. Nat Electron 2020;3:571–8.
[18] Wang J, He T, Lee C. Development of neural interfaces and energy harvesters towards self-powered implantable systems for healthcare monitoring and rehabilitation purposes. Nano Energy 2019;65:104039.
[19] Hinchet R, Kim SW. Wearable and implantable mechanical energy harvesters for self-powered biomedical systems. ACS Nano 2015;9:7742–5.
[20] Wang H, Wang J, He T, et al. Direct muscle stimulation using diode-amplified triboelectric nanogenerators (TENGs). Nano Energy 2019;63:103844.
[21] Shan Y, Feng H, Li Z. Electrical stimulation for nervous system injury: research progress and prospects. Acta Phys Chim Sin 2020;36:2005038.
[22] Luo R, Dai J, Zhang J, et al. Accelerated skin wound healing by electrical stimulation. Adv Healthc Mater 2021;10:2100557.
[23] Zhang Y, Xu L, Liu Z, et al. Self-powered pulsed direct current stimulation system for enhancing osteogenesis in MC3T3-E1. Nano Energy 2021;85:106009.
[24] Conta G, Libanori A, Tat T, et al. Triboelectric nanogenerators for therapeutic electrical stimulation. Adv Mater 2021;33:2007502.
[25] Wang H, Wu TZ, Zeng Q, et al. A review and perspective for the development of triboelectric nanogenerator (TENG)-based self-powered neuroprosthetics. Micromachines 2020;11:865.
[26] Schuepbach WM, Rau J, Knudsen K, et al. Neurostimulation for Parkinson's disease with early motor complications. N Engl J Med 2013;368:610–22.
[27] Stavrakis S, Humphrey MB, Scherlag BJ, et al. Low-level transcutaneous electrical vagus nerve stimulation suppresses atrial fibrillation. J Am Coll Cardiol 2015;65:867–75.
[28] Zhong Y, Wang Y, He Z, et al. Closed-loop wearable ultrasound deep brain stimulation system based on EEG in mice. J Neural Eng 2021;18:0460e8.
[29] Opri E, Cernera S, Molina R, et al. Chronic embedded cortico-thalamic closed-loop deep brain stimulation for the treatment of essential tremor. Sci Transl Med 2020;12:eaay7680.
[30] Ouyang Z, Sperry ZJ, Barrera ND, et al. Real-time bladder pressure estimation for closed-loop control in a detrusor overactivity model. IEEE Trans Neural Syst Rehabil Eng 2019;27:1209–16.
[31] Ouyang H, Tian J, Sun G, et al. Self-powered pulse sensor for antidiastole of cardiovascular disease. Adv Mater 2017;29:1703456.
[32] Zou D, Geng N, Chen Y, et al. Ranolazine improves oxidative stress and mitochondrial function in the atrium of acetylcholine-$CaCl_2$ induced atrial fibrillation rats. Life Sci 2016;156:7–14.
[33] Fu Y, Jiang T, Sun H, et al. Necroptosis is required for atrial fibrillation and involved in aerobic exercise-conferred cardioprotection. J Cell Mol Med 2021;25:8363–75.
[34] Shi Y, Liu R, He L, et al. Recent development of implantable and flexible nerve electrodes. Smart Mater Med 2020;1:131–47.
[35] Zhang W, Liu Q, Chao S, et al. Ultrathin stretchable triboelectric nanogenerators improved by postcharging electrode material. ACS Appl Mater Interfaces 2021;13:42966–76.
[36] Fang Y, Zou Y, Xu J, et al. Ambulatory cardiovascular monitoring via a machine-learning-assisted textile triboelectric sensor. Adv Mater 2021;33:2104178.

[37] Zhang S, Bick M, Xiao X, et al. Leveraging triboelectric nanogenerators for bioengineering. Matter 2021;4:845–87.
[38] Chao S, Ouyang H, Jiang D, et al. Triboelectric nanogenerator based on degradable materials. EcoMat 2020;3:e12072.
[39] Li H, Zhao C, Wang X, et al. Fully bioabsorbable capacitor as an energy storage unit for implantable medical electronics. Adv Sci 2019;6:1801625.
[40] Zou Y, Tan P, Shi B, et al. A bionic stretchable nanogenerator for underwater sensing and energy harvesting. Nat Commun 2019;10:1–10.
[41] Sha Y, Scherlag BJ, Yu L, et al. Low-level right vagal stimulation: anticholinergic and antiadrenergic effects. J Cardiovasc Electrophysiol 2011;22:1147–53.
[42] Shen MJ, Hao-Che C, Park HW, et al. Low-level vagus nerve stimulation upregulates small conductance calcium-activated potassium channels in the stellate ganglion. Heart Rhythm 2013;10:910–5.
[43] Stavrakis S, Scherlag BJ, Fan Y, et al. Inhibition of atrial fibrillation by low-level vagus nerve stimulation: the role of the nitric oxide signaling pathway. J Interv Card Electrophysiol 2013;36:199–208.
[44] Friedman DJ, Chasten T, Anderson K, et al. Premature ventricular contraction response-induced new-onset atrial fibrillation. HeartRhythm Case Reports 2019;5:120–3.
[45] Kato T, Iwasaki YK, Nattel S. Connexins and atrial fibrillation: filling in the gaps. Circulation 2012;125:203–6.
[46] Diao SL, Xu HP, Zhang B, et al. Associations of MMP-2, BAX, and Bcl-2 mRNA and protein expressions with development of atrial fibrillation. Med Sci Monit 2016;22:1497–507.
[47] Li Y, Song B, Xu C. Effects of Guanfu total base on Bcl-2 and Bax expression and correlation with atrial fibrillation. Hellenic J Cardiol 2018;59:274–8.
[48] Hu YF, Chen YJ, Lin YJ, et al. Inflammation and the pathogenesis of atrial fibrillation. Nat Rev Cardiol 2015;12:230–43.
[49] Yu L, Scherlag BJ, Li S, et al. Low-level vagosympathetic nerve stimulation inhibits atrial fibrillation inducibility: direct evidence by neural recordings from intrinsic cardiac ganglia. J Cardiovasc Electrophysiol 2011;22:455–63.
[50] Ouyang H, Jiang D, Fan Y, et al. Self-powered technology for next-generation biosensor. Sci Bull 2021;66:1709–12.
[51] Xiang S, Liu D, Jiang C, et al. Liquid-metal-based dynamic thermoregulating and self-powered electronic skin. Adv Funct Mater 2021;31:2100940.
[52] Tang Y, Zhou H, Sun X, et al. Triboelectric touch-free screen sensor for noncontact gesture recognizing. Adv Funct Mater 2019;30:1907893.

Yu Sun received his Bachelor's degree from Anhui Medical University of Clinical Medicine in 2019. He is currently pursuing his Master's Degree of Surgery at Anhui Medical University. His research work mainly focuses on closed-loop neuromodulation and diagnosis and treatment of cardiovascular diseases.

Shengyu Chao received his Bachelor's degree from Dalian University of Technology in 2018. He is currently pursuing his Ph.D. degree at Beijing Institute of Nanoenergy and Nanosystems, Chinese Academy of Sciences. His research work mainly focuses on triboelectric generator, electrical stimulation devices and related biological effects.

Jun Yang is professor and chief physician of Peking University. He had studied as a visiting scholar at the World's Neurosurgery Center-Phoenix BNI, USA, and Hannover INI, Germany in the groups of Profs. Spetzler and Sami respectively. His research is mainly engaged in basic and clinical research on skull base lesions and brain tumors, cerebrovascular, spinal cord and functional neurosurgery.

Hongqing Feng received her Doctor's Degree at Peking University. She is currently working as an associate professor at Beijing Institute of Nanoenergy and Nanosystems, Chinese Academy of Sciences. Her research interest includes anti-bacterial technologies and the biomedical applications of nanogenerators.

Gengsheng Mao received his M.D. degree from the Tianjin Medical University in 2006 and received his postdoctoral training at Capital Medical University. Currently, he is the chief physician of Neurosurgery at the Third Medical Center of the General Hospital of the People's Liberation Army and a professor at Anhui Medical University. His research interest includes the diagnosis and treatment of a variety of neurosurgical diseases, especially in the operation and interventional treatment of cerebrovascular diseases.

Zhou Li received his Ph.D. degree from Department of Biomedical Engineering, Peking University in 2010, and Bachelor's Degree from Wuhan University in 2004. He joined School of Biological Science and Medical Engineering, Beihang University in 2010 as an associate professor. Currently, he is a professor at Beijing Institute of Nanoenergy and Nanosystems, Chinese Academy of Sciences. His research interest includes nanogenerators, *in vivo* energy harvesters, self-powered medical devices, and biosensors.